

# On the Effects of Industrial Robotic Arms on the Pattern of the Probe for Near-Field Measurements

Vince Rodriguez<sup>1</sup>, FELLOW, AMTA, P. Mark Ingerson<sup>1</sup>, Gwenael Dun<sup>2</sup> and Esra Celenk<sup>1</sup>

(1) EM ANALYSIS GROUP, NSI-MI TECHNOLOGIES, SUWANEE, GEORGIA, U.S.A.

(2) EM Analysis Group, NSI-MI Technologies, C/O AMETEK SAS, Elancourt, France.

**Abstract**—The first mention of a Robot for near-field measurements of antennas appears is by Jeff Snow in [1]. This was a simple robotic arm to do planar measurements. About 7 years later, the use of off-the-shelf industrial robotic arms for doing antenna measurements is introduced [2]. Since then, industrial-robot-arm based antenna measurement systems have become increasingly popular due to their flexibility to measure over different surfaces allowing the system to do planar, spherical and cylindrical. The use of other methods to perform the transform, by numerically compute the currents on an arbitrary surface from the measured fields has helped in the growing popularity of robotic systems. This is related that the measurement surface does no longer have to be a canonical surface but can be any shape. However, the flexibility of the robots may be limited by the RF absorber coverage used in treating them. In this paper, the authors explore the potential scattering from the robotic arm in different positions and its effect on the probe illuminations. This is an area of research on the use of absorber that has not been explored until recently [3]. Numerical experiments are conducted to explore the effects of RF absorbers in the 300 MHz to 3 GHz range. Open ended waveguides (OEWG) as well as dual ridged horns (see Figure 1) are used as the probes. The results suggest that some areas of the arm need to be treated while others can be left bare. The analyses performed suggest that optimized treatment of robotic arms to maintain the flexibility of the technique while also reducing effects on the probe illuminations are possible.

**Index Terms**—Antenna Measurements, Computational Electromagnetics, Near-Field, RF-Absorbers, Robotic Systems

## I. INTRODUCTION

While off-the-shelf industrial robot arms have become increasingly popular for near-field antenna measurements as well as for their use in positioning antennas for extrapolation gain measurements [4]. The amount of publications on the subject has exploded in the past 5 years. National metrology laboratories [4, 5] as well as academic institutions [6,7]. are using robotic arms in their services and research. But on all these papers while there is a lot of work on non-canonical surface techniques or data acquisition minimization, there is little information on absorber treatment for the robotic arms. Sometimes robots are treated with a huge amount of absorber that hinders their movement and takes away from their flexibility to perform measurements over very complex surfaces. Recently the authors presented a paper where it was shown that the forearm of the robot does not need to be treated [3]. In this paper further analysis of the robot is performed to provide some guidance on the treatment of the upper arm which was shown in [3] to require treatment in some orientations to minimize effects on the probe

illumination. In this paper the same analysis approach used in [3] is continued but more of the joints of the robot that were omitted in the previous work are introduced now. These include the shoulder joint and the supporting pedestal. The full model is shown in Figure 1.



Figure 1: A dual ridged antenna is used as a broadband probe with an industrial robotic arm. The model is rotated to study the effect of the arm on the probe illumination at different arm positions.

## II. ELECTROMAGNETIC ROBOT AND PROBE MODELS

The model in Figure 1 is an approximation to a typical off-the-shelf industrial robot arm. The entire model is assumed to be perfect electric conductor (PEC). The model is also simplified to minimized the number of quadrilateral patches required for solving the geometry in the method of moments. The numerical commercial tool used is the same used in [8,9] where a traditional AUT positioner was analyzed. Figure 2 shows the overall geometry of the robot model. The size and shape is an approximation to off-the-shelf industrial robots. The model fixes the position of the probe to the global coordinate system and rotates the arm around it to mimic the probe being positioned by the arm. This approach allows the software to compute the field around the probe with the robot arm and easily compare it to the fields from the probe by itself. If the fields in the presence of the robot arm are defined as the total field ( $\mathbf{E}^T$ ) and the field from the probe by itself are defined as the incident field ( $\mathbf{E}^I$ ), then the scattered field generated by the presence of the robotic arm can be computed by using the equation (1):

$$\mathbf{E}^S = \mathbf{E}^T - \mathbf{E}^I \quad (1)$$

### III. SCATTERED FIELD FROM ROBOT ARM

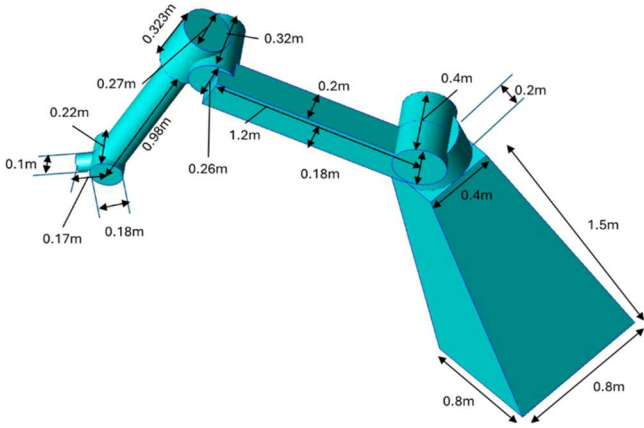


Figure 2: Geometry of the robot arm without the probe mounted.

The level of the scattered field computed using equation (1) provides an indication of the effect of the robot on the probe illumination. The two probes analyzed are the same as those used in [3]. For the lower frequencies (300MHz and 500MHz) a dual ridge horn antenna (DRHA) described in MIL STD 461G as the antenna required for 200MHz to 1 GHz RE102 testing (see section 5.18.3.2 of [10]) is used. For 2.75 GHz an open ended waveguide (OEWG) WR-340 probe is used. The DRHA has a 18-inch (45 cm) pyramidal absorber collar behind it with a 0.61 m by 0.61m in size. The OEWG has an absorber collar of 12-inch (30.5 cm) absorber cut in circle of 0.61m diameter. Figure 3 shows the models for these two probes.

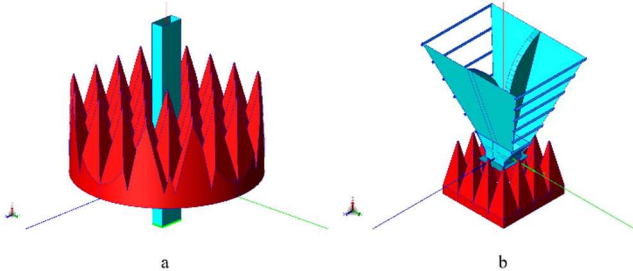


Figure 3: Models for the OEWG (a) with the absorber collar, and a dual ridge horn antenna (b) with the absorber treatment.

The probes in Figure 3 were simulated and the near fields around were computed. The field was computed on the plane where the electric field is oriented (effectively the E plane of the antenna). The field was computed on a 4m by 4m plane. the field was computed every 0.01 m. at every point the complex field for each of the three orthogonal components was computed. The field is computed at the same points when the arm is present and then the scattered field is computed using (1). Figure 4 shows the magnitude of the incident field for each of the two probes at 300MHz and 500MHz for the DRHA and 2.75 GHz for the OEWG. The distributions, although in the near field do resemble the radiation patterns of these probes as reported in reference [3].

In reference [3] it was shown that the worst case for reflections from the forearm of the robot arose when the field was co-polarized with the length of the arm. The largest effect on the illumination of the probe was when the upper arm of the robot was next to the probe (See figure 5). However, At the lower frequencies simulated (300MHz and 500 MHz) the effect reported was minimal. Scattered fields were 50dB lower than the incident field for the 500MHz case in the region extending  $3.3 \lambda$  from the probe (i.e. about 2 meters). This was also related to the beamwidth of the probe, as for 300MHz, the scattered fields were more than 40dB lower than the incident field. In the same region (about  $2 \lambda$  at 300MHz). Figure 5 shows the field distribution with the robot arm next to the probe aligned to the main E field. Comparing the field distributions in Figure 5, the total field, to the field distributions on Figure 4 (the incident field), it is very obvious that at these low frequencies the effect of the arm is minimal and therefore there is no RF absorber required. However, as the frequency increases to the upper end of the VHF band, the effect of the arm is significant. There it is clear, that RF absorber is needed to mitigate the effects from the arm. Even that the effect is clearly visible, Reference [3] showed that the level of scattered field at 2.75 GHz from the untreated robot arm was about 18 dB lower than the incident field. Thus, absorber with a bi-static reflectivity of -20 dB will suffice to treat the arm. In reference [11], it is shown that  $0.6\lambda$  absorber will provide better than -20 dB up to 30 degrees off-normal incidence. At 2.75 GHz means that 3-inch pyramidal absorber will suffice.

### IV. SCATTERED FIELD FROM ROBOT PEDESTAL

In the present paper the “shoulder”, consisting of two additional axes of rotations is included in the simulations. The shoulder is mounted onto a pedestal to raise it up above the floor of the range. This pedestal shown in Figure 2, is a truncated pyramid with a square base having a dimension of 0.8 m per side and a height of 1.5 meters. The top of this truncated pyramid is a square with 0.4 m per side onto which an azimuth stage is placed. This azimuth stage is part of the robotic arm shoulder. The pedestal is not part of the robot, but it is typically added by the system integrator to position the arm mid height inside the anechoic range to allow for the robot to position the probe above the antenna under test.

The shape of the pedestal, is chosen to make it easier to treat with RF absorber pieces, hence the flat facets. In Figure 6. The geometry of the robot is shown with the pedestal with the OEWG probe and the DRHA facing the floor having the pedestal oriented two different ways. Figure 6a shows the DRHA with a flat side of the pedestal facing the probe, while Figure 6c shows the probe facing an edge of the pedestal (the robot has rotated 45 degrees). Figure 6b and Figure 6d show the same geometries when the probe is an OEWG.

The results of these simulations are shown on Figure 7 through 9. The total and scattered fields are shown for the different frequencies and geometries of the robot shown in Figure 6.

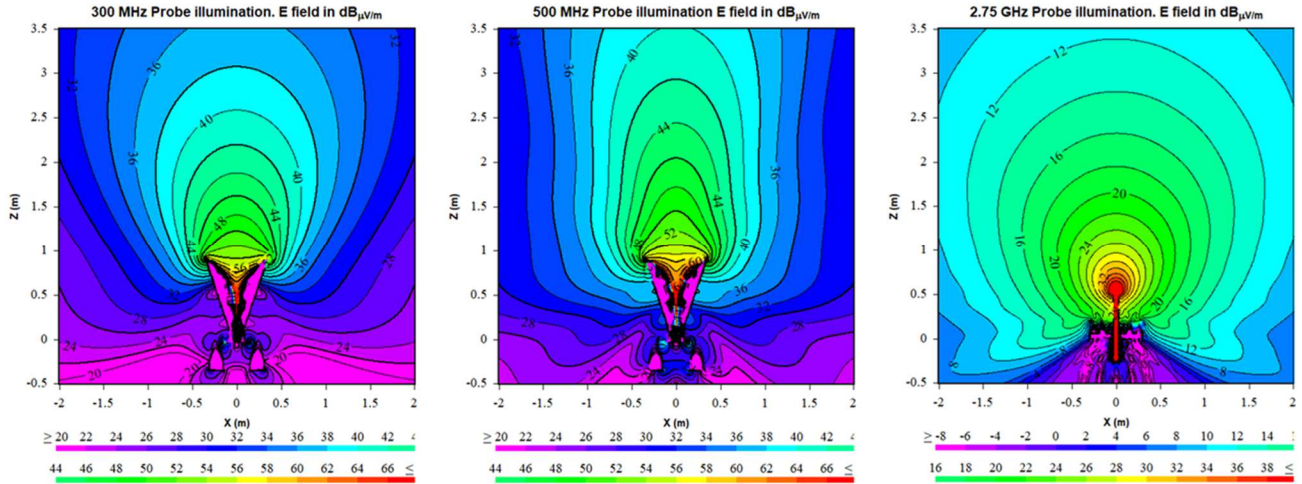


Figure 4: Illumination on the E plane from the probes in the near field without the robot arm. This is effectively the incident field  $\mathbf{E}^I$  used in the calculations for the scattered field from the robot arm [3].

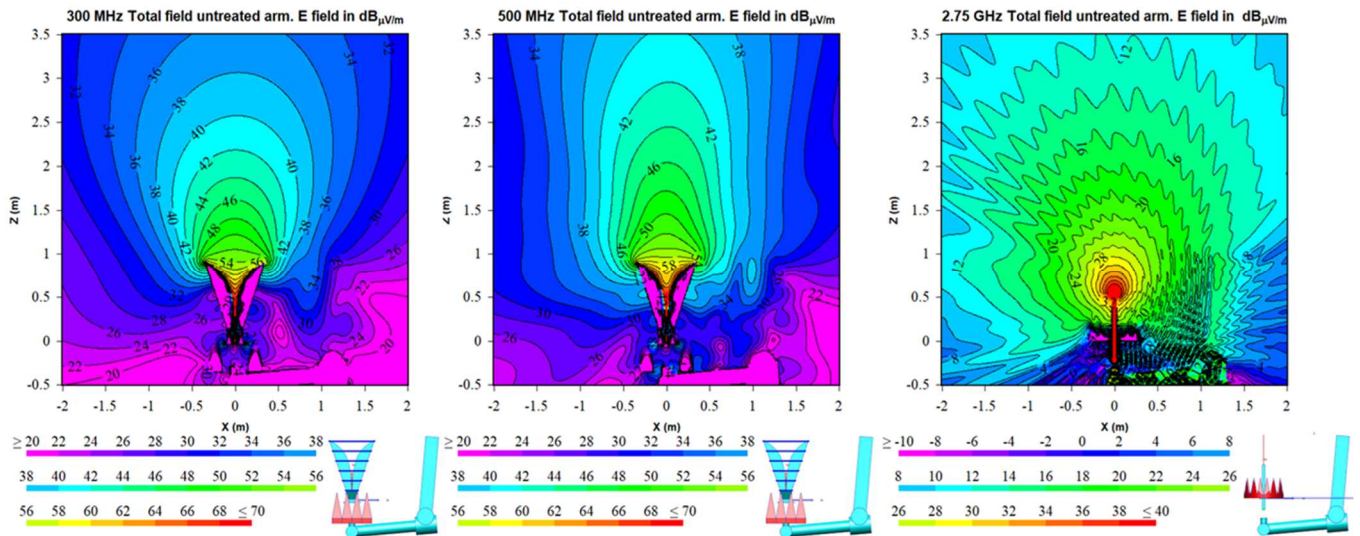


Figure 5: Illumination on the E plane from the probes in the near field with the upper arm of the robot untreated next to the probe,  $\mathbf{E}^T$ . These results were reported in [3].

In Figures 7 through 9, the location of the absorber treated floor is shown with a white line. There is no absorber modeled as it is assumed that a perfect absorber exists. This is the same approach taken in [8, 9] to isolate the effects of the AUT positioner. Here the assumption of a perfectly absorbing floor is used to isolate the effects of the robot on the probe illumination to better understand its levels and also to better understand the necessary RF absorber treatment required. Figure 7 shows the results at 300 MHz. The computed results for 500 MHz are shown in Figure 8. The results in Figure 9 are for the WR-340 OEWG

in Figure 7 the four plots show the total and the scattered fields for the geometry shown on figure 6a and figure 6b. The

plots on the left show the figure 6a results. Those are cases where the flat surface of the pedestal faces the probe. The effect of the pedestal is apparent on the total field. The side closer to the pedestal is affected by its presence. High scattered fields are present between the pedestal and the probe. Results show that in front of the probe the scattered fields are about 28 dB lower than the incident fields shown on Figure 4. When the robot rotates 45 degrees with respect to the pedestal so that the probe is adjacent to the edge of the pedestal (Figure 6c) the effect of the pedestal on the illumination is reduced. This can be seen on the total field plot, but also on the scattered field where the magnitude of the scattered field in front of the probe is much smaller with levels in excess of 32 dB lower than the incident fields plotted in figure 4.

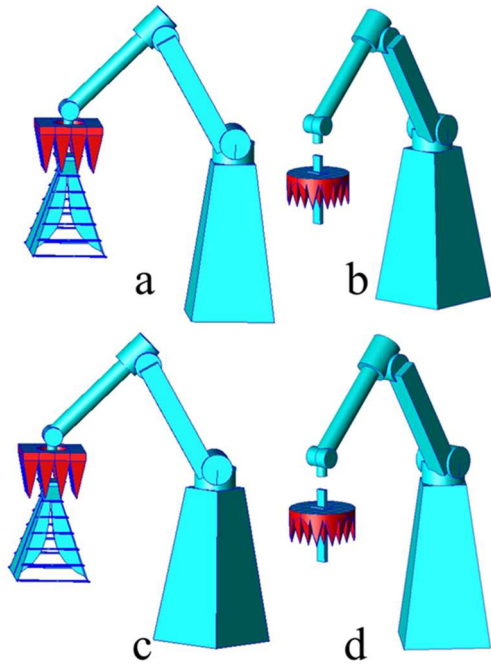


Figure 6: Different geometries of the robot arm to check the effect of the pedestal that supports the robot.

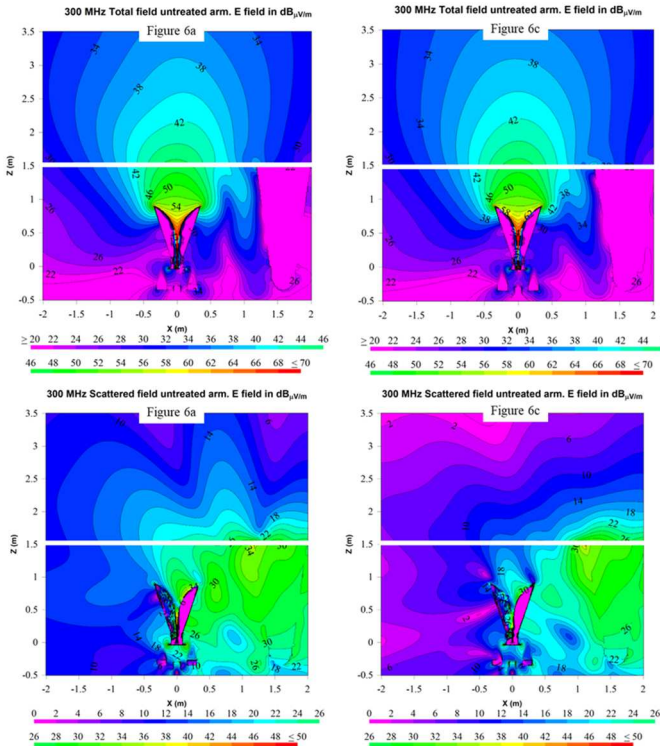


Figure 7: Field distribution  $E^T$  and  $E^S$  at 300 MHz for the DRHA probe for the geometries in Figure 6.

The results for 500 MHz shown on Figure 8 also are similar to the results on Figure 7 for 300 MHz, for the geometry of figure

6a where the DRHA probe is adjacent to a flat surface (plots on the left on Figure 8) the scattered field is stronger, this can be seen on the total field plots where the distribution is more affected for the case with the flat surface than for the case where the pedestal is rotated 45 degrees. In Figure 8 there is a very clear standing wave between probe and pedestal. The standing wave is not that well defined in the case where the robot is rotated 45 degrees in relation to the pedestal. For the case in Figure 6a, (the flat face) the scattered fields in front of the DRHA probe are about 20 dB lower than the incident field. But for the case on Figure 6c, the fields are about 30 dB lower.

These analyses of the DRHA show that the shape of the pedestal is critical, and potentially truncated conical pedestals should be used to minimize the differences in scattering from the pedestal as the robot rotates in azimuth about its “shoulder”. These results show that at least 12-inch (30.5 cm) pyramidal absorber should be used on the pedestal flat surfaces. Reference [11] showed that  $0.5 \lambda$  pyramidal absorber will provide at least 15 dB of attenuation which should be enough to reduce the scattering to the -35 to -45 dB level. While not extremely large, that absorber is a significant size that may reduce the overall movement and flexibility of the robot to avoid the collision between probe and absorber.

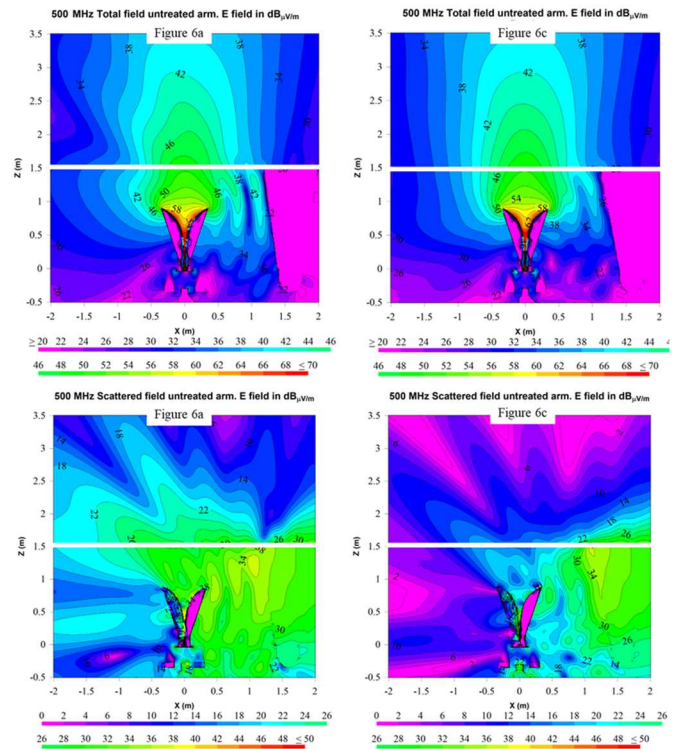


Figure 8: Field distribution  $E^T$  and  $E^S$  at 500 MHz for the DRHA probe for the geometries in Figure 6.

Finally in Figure 9, the results for the WR-340 OEWG probe at 2.75 GHz are shown for the geometries shown on Figure 6b and Figure 6d. As was the case for the DRHA probe at 300 and 500 MHz, the cases where the probe is adjacent to the flat face of the pedestal show a significantly higher scattering. This is clear even in the plots of the total field. The scattering field plots also show

that the levels are higher for the flat face facing the probe as expected based on the total field probes.

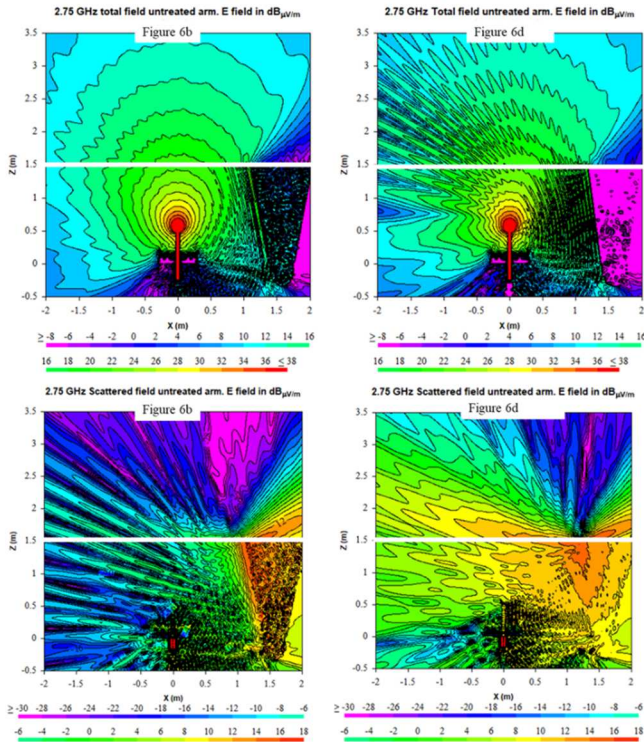


Figure 9: Field distribution  $E^T$  and  $E^S$  at 2.75 GHz for the OEWG probe for the geometries in Figure 6.

Scattering field levels for the geometry in Figure 6b are about 10dB lower than the incident field shown on Figure 4. While for the case shown in Figure 6d, the scattering field levels are about 20 dB lower than the incident fields. Based on these results an absorber treatment that would provide -30 dB of reflectivity would be required to reduce the scattered field to a -40dB level. Reference [11] shows that absorber about  $1\lambda$  in size will be required to treat the pedestal, which at 2.75 GHz is about 4-inches (10 cm) pyramidal absorber. However it is strongly encourage to shape the pedestal to avoid the flat surfaces facing the probe.

## V. CONCLUSIONS

It has been shown that numerical methods can be used to estimate the scattering levels from industrial robotic arms. The methodology is a good approach to analyze robot type structure and optimize the absorber coverage so that the flexibility of the robot arm solution is not affected by the absorber treatment. The

results have supported what was found in [3] where little absorber is required at lower frequencies. This makes the robot a feasible solution as large pyramidal absorber treatment is not required to cover the surfaces of the robot.

The typical truncated pyramid pedestal used is not an ideal shape as its scattering changes significantly as the probe is oriented around it. Scattered fields at 2.75 GHz changed from 20 to 10 dB below the incident field A truncated cone may be a better shape with a small coating of absorber to further reduce the scattering levels.

## REFERENCES

- [1] J. Snow and W. Slowey “SCARA Scanner for Portable Near-Field Antenna Testing” *27th Annual Symposium of the Antenna Measurement Techniques Association AMTA 2005*, Newport RI, November 2005.
- [2] J. Gordon, D. Novotny, et al “Robotically Controlled mm-Wave Near-Field pattern range” *34th Annual Symposium of the Antenna Measurement Techniques Association AMTA 2012*, Bellevue WA, October 2012.
- [3] V. Rodriguez, P. M. Ingerson, E. Celenk and G. Dun “Requirement of RF Absorber Coverage for Industrial Robotic Arms Used in UHF Antenna Measurements” *2025 IEEE International Symposium on Antennas & Propagation and North American Radio Science Meeting*, Ottawa, Canada, 12-18 July 2025.
- [4] J. Gordon and B. Moser “NIST Antenna Gain and Polarization Calibration Service Reinstatement” *45th Annual Meeting and Symposium of the Antenna Measurement Techniques Association AMTA 2023*, Seattle, WA, USA. October 8-13, 2023.
- [5] J-Y Kwon, W. Jung, and S. Lee “Application-orientated Robot-based Precision Antenna Measurement System” *46th Annual Meeting and Symposium of the Antenna Measurement Techniques Association AMTA 2024*, Cincinnati, OH, WA, USA. Oct 27-Nov 1, 2024.
- [6] F. Rodríguez Varela, A. Arboleya, E. Martínez-de-Rioja, C. Fontá Romero, and M. Sierra Castañer “Robotic Near-Field Measurements using Reduced Angular Sparse Grids” *46th Annual Meeting and Symposium of the Antenna Measurement Techniques Association AMTA 2024*, Cincinnati, OH, WA, USA. Oct 27-Nov 1, 2024.
- [7] H. Jansen, R. Moch, and D. Heberling “Reduction of Multiple Reflections Through Intentional Probe Tilting Enabled by Robot-Based Measurement Systems” *46th Annual Meeting and Symposium of the Antenna Measurement Techniques Association AMTA 2024*, Cincinnati, OH, WA, USA. Oct 27-Nov 1, 2024.
- [8] V. Rodriguez, M. Ingerson and G. Dun, "On the RF Absorber Coverage of Antenna under Test Positioners," *2024 18th European Conference on Antennas and Propagation (EuCAP)*, Glasgow, United Kingdom, 2024, pp. 1-5, doi: 10.23919/EuCAP60739.2024.10501680.
- [9] M. Ingerson, G. Dun and V. Rodriguez, "Effects of Antenna Under Test Positioner on the Measured Pattern of Antennas," *2024 IEEE International Symposium on Antennas and Propagation and INC/USNC - URSI Radio Science Meeting (AP-S/INC-USNC-URSI)*, Firenze, Italy, 2024, pp. 1835-1836, doi: 10.1109/AP-S/INC-USNC-URSI52054.2024.10686623.
- [10] MIL-STD-461G, Requirements for the Control of Electromagnetic Interference Characteristics of Subsystems and Equipment, 11 December 2015, Department of Defense.
- [11] V. Rodriguez, *Anechoic Range Design For Electromagnetic Measurements*, Artech, 2019.